Elsevier Editorial System(tm) for International Journal of Plasticity
Manuscript Draft

Manuscript Number:

Title: The Effect of Dynamic Plasticity on the Crack Propagation in Thin Plates Subjected to Impact Loading

Article Type: Research Paper

Keywords: Crack Propagation, Plastic Zone Size, Elastoplastic Stress Field, Elastoplastic Strain Field, Experimental Plastic Strain, Impact Loading, Elastoplastic Stress Intensity Factors

Corresponding Author: Mr. Muthenna Abdul-Hussein Ali, -

Corresponding Author's Institution: Baghdad University

First Author: Muthenna A Ali, Researcher

Order of Authors: Muthenna A Ali, Researcher; Fathy A Al-Shamma, Assistant Professor

Abstract: In the present study an investigation upon simply-supported thin plates having surface cracks within their structure is to be accomplished, and the applied impact load to these thin plates tends to induce infinite stresses and strains at the crack tip of the existing cracks. Extensions of these cracks may be evolved from the crack tip, and the cracks may propagate in a specified path with certain velocities. At the same instant, yielded zones are emanated around the crack tip due to occurrence of the impact load. Two methods of computation are utilized here; the first one is the analytical method which is derived from the classical plate theory, whose concepts are illustrating the required expressions of plane stress conditions for thin plates, taking into consideration the effects of impact loading in conjunction with the elastoplastic fracture mechanics and dynamic crack growth concepts. The second technique is the experimental analysis using the grid method (remeshing technique); so as to measure the permanent strains induced within the grid points within the plates. Finally, a total solution leads to the arrival at the analytical and experimental results concerning the crack-development speed, plastic-zone size, and the crack-tip-nearby elastoplastic stress and strain fields.

The Effect of Dynamic Plasticity on the Crack Propagation in Thin Plates Subjected to Impact Loading

Muthenna Abdul-Hussein Ali

Mechanical Engineering Department – Baghdad University – Al-Jadiriyah – Baghdad – Iraq

+9647901831234

Muthenna_rockstar@yahoo.com

Fathy Abdul-Sahib Al-Shamma

Mechanical Engineering Department – Baghdad University – Al- Jadiriyah – Baghdad – Iraq

+9647810846720

Fathi-Alshamma@yahoo.com

Highlights

- Utilizations of the plate-theory considerations and the impact-load nature in conjunction with the elastoplastic-fracture-mechanics concepts are to be elaborated for the present mathematical model.
- An implementation of a finite-dimensions grid upon the elastoplastically-deformed cracked plates is achieved to measure the permanently-induced displacements.
- A remarkable contrast between the crack-growth-speed values and the around-crack-tip plastic-zone extensions is to be investigated.
- We process the crack-tip-nearby stress and strain fields' behavior for the linear elastic-ideally plastic-based cracked plates.

Nomenclature:

Symbol	Description	Units
A	Contact Area between the Plate Surface and the Striking Bullet	m^2
a	Plate Width	cm
a_c	The Critical Crack Length	mm
a_{cr}	Characteristic Crack Length	mm
$\dot{a}_{cr}$	Speed of the Crack Propagation	m/s
a_0	The Existing Crack Length within the Thin Plates	mm
AR	Plate Aspect Ratio	-
b	Length of the Thin Plate	cm
c	Plastic Zone Size	mm
d	Distance between the Pistol and the Thin Plate Where the Velocity of Bullet Becomes Zero	m
E	Modulus of Elasticity	Mpa
$F(t)$	Time-Dependent Impacting Force	N
G	The Energy Release Rate	N
g	Gravitational Acceleration of Earth	m/s^2
h	The Thickness of the Plate	mm
K_I	The Elastic Stress Intensity Factor	$Mpa.\sqrt{m}$
$K_{I,ep}$	The Elastoplastic Stress Intensity Factor	$Mpa.\sqrt{m}$
M_x	X-Axis Bending Moment	$N.m$
M_y	Y-Axis Bending Moment	$N.m$
m_o	Mass of the Copper-Covered Bullets	kg
P_o	Contact Pressure between the Thin Plate Surface and the Impacting Bullets	Mpa
R	The Crack Resistance	N
r	The Variable Radial Position	mm

t	The Time Duration of Contact between the Thin Plate and the Striking Bullet	μs
$\begin{bmatrix} u_x \\ u_y \end{bmatrix}_{ep}$	Elastoplastic Displacement Field near the Crack Tip	μm
v_1	Muzzle Velocity of the Bullets Exiting from the Pistol	m/s
x	The Horizontal Distance along the Thin Plate	m
y	The Vertical Distance along the Thin Plate	m
ε_{xx}	Normal Strain along the X-Axis	-
ε_{yy}	Normal Strain along the Y-Axis	-
γ_{xy}	Shear Strain	-
$\begin{bmatrix} \varepsilon_{xx} \\ \varepsilon_{yy} \\ \gamma_{xy} \end{bmatrix}_{ep}$	Elastoplastic Strain Field near the Crack Tip	-
η	The Vertical Distance Where the Load Acts	m
θ	The Variable Angular Position	deg
ν	Poisson's Ratio	-
ξ	The Horizontal Distance Where the Load Acts	m
σ_Y	Yield Stress	Mpa
σ_{xx}	Normal Stress along the X-Axis	Mpa
σ_{yy}	Normal Stress along the Y-Axis	Mpa
τ_{xy}	Shear Stress	Mpa
$\begin{bmatrix} \sigma_{xx} \\ \sigma_{yy} \\ \tau_{xy} \end{bmatrix}_{ep}$	Elastoplastic Stress Field near the Crack Tip	Mpa

1. Introduction:

Of a particular concern within the present work is to study the solid body, whose structure is experiencing large deformations and loss of contact between parts of the solid body itself, undergoing extreme loading which leads to the elastoplastic deformation with or without the occurrence of the total fracture. As a contributing fact, fracture may be evolved before, after, or in conjunction with the occurrence of the large deformation process **[7]**.

During the last few decades, a number of oil cargo ship failures have contributed to cascade oil into rich fishing regions and coastal beach areas as well as the collision of the passenger liner *Titanic* with a large iceberg causing it to experience brittle fracture with its parts and killing about 1500 passengers and crew members, as a consequence, all the solid structures are to be susceptible to the same fate. Therefore, design analysts should be familiar with the fact that the fracture phenomenon is regarded to be one of the most dangerous defects undergone by a solid body **[16]**. The stress concentrations within fractured or collapsed structures, the existence of flaws, microcracks, or sharp notches, and the capability of cracks to traverse throughout the structures are all cited as the contributing factors in the fracture phenomenon.

To be investigated within the current research are crack-tip-nearby elastoplastic stress and strain fields, extents of the yielded zone around the crack tip, and the crack-development speeds analytically and experimentally for simply-supported cracked thin plates, which have different aspect ratios (1, 1.334, and 2), crack lengths (10, 20, and 30 mm), and plate alloy types (pure aluminum 1100 and aluminum-copper 2014 alloy types), under theoretically-assumed triangular-type impacting load **[17].**

The upcoming researches are elaborated so as to support the outlining subjects of the current research, which are to be cited within the dynamic crack propagation and fracture mechanics concepts, plastic strain and plastic-zone size evaluation procedures, impact loading of thin plates topics, and elastoplastic stress intensity factor formulations.

M. Krawczuk, M. Palacz, and W. Ostachowicz (2004) **[10]** achieved their research in order to present the method of analysis of the wave propagation process in cracked plates. For modeling the plate new type of finite spectral plate element with a crack was elaborated. It was assumed that the crack having an arbitrary length, depth and location was parallel to one side of the plate. Elastic behavior of the plate at the crack location was considered as a line spring with a varying stiffness along the crack length.

G. G. Corbett, S. R. Reid, and W. Johnson (1996) **[3]** have reviewed recent research into the penetration and deformation of plates and cylinders by free-flying projectiles travelling at sub-ordnance velocities. It is shown that over the last few years there has been a significant amount of experimental research into a wide range of projectile-target configurations. Although most of this research has been concerned with the normal impact of monolithic metallic plates by non-deformable projectiles, valuable work has also been carried out on non-normal impact, impact by deformable projectiles (including bullets of various guns which is used during the experiment), impact of non-homogeneous metallic and non-metallic targets (including laminated targets) and impact of pipes and tubes.

D. S. Dugdale (1960) **[2]** has investigated the yielding undergone at the end of a surface or through (internal) slit in a sheet by an external load, and obtained a relation between the extent of the plastic yielding and the external load applied. To verify this relation, panels containing internal and edge slits were loaded in tension and lengths of plastic zones were measured. The elastic stress intensity factors are normalized dynamically for ductile materials into elastoplastic stress intensity factors, in order to distinguish how much stresses and strains near the crack tip and speeds of the propagating cracks for an elastic-ideally plastic Tresca material which is experiencing an external load.

J. H. Underwood and D. P. Kendall (1969) **[5]** have utilized two independent experimental techniques so as to measure the strain distribution within the plastically deformed region around a crack tip. By using a microscope, permanent plastic deformations near the crack tip are investigated and it is compared with the method of Moiré grid

interference which is used to measure the in-plane strain with the specimen grid engraved directly on the specimen surface. The testing arrangement allows measurement of at-load strain as well as residual strain. The measured strain distribution is compared with recent work by Swedlow using a finite-element numerical technique and with results of the etch-pit technique used by Hahn and Rosenfield.

2. Analytical Approach:

2.1 The Mathematical Model: Elastoplastic Stress and Strain Fields and Dugdale's Approach:

The mathematical model of a cracked thin plate is shown in Fig. (1), the following underlying assumptions are adequately convenient to utilize in order to arrive at the final analytical expressions: the plate is thin enough for plane stress to occur, isothermal conditions are assumed for the linearly isotropic continuum, i.e., any temperature change during the impact process is of no concern within the present illustration, and the impacted-plate alloy type is homogenous and of a linearly-elastic-ideally-plastic behavior whose yield limit can be approximated, with fairly good results, by Tresca's failure criterion. Hence, proceeding from the plane-stress-based equilibrium equations for a solid medium, small-strain-theory-based kinematic constraints, and for-linearly-isotropic-alloy-type Hooke's law **[7]**

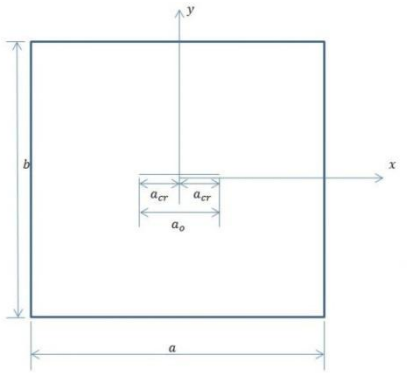

Fig. (1) The Centrally-Cracked-Plate Mathematical Model

$$\frac{\partial \sigma_{xx}}{\partial x} + \frac{\partial \tau_{xy}}{\partial y} = 0$$
$$\frac{\partial \tau_{xy}}{\partial x} + \frac{\partial \sigma_{yy}}{\partial y} = 0 \quad \dots\dots\dots\dots\dots\dots (1)$$

$$\varepsilon_{xx} = \frac{\partial u_x}{\partial x}$$
$$\varepsilon_{yy} = \frac{\partial u_y}{\partial y} \quad \dots\dots\dots (2)$$
$$\gamma_{xy} = \frac{\partial u_x}{\partial y} + \frac{\partial u_y}{\partial x}$$

$$\varepsilon_{xx} = \frac{1}{E}\left(\sigma_{xx} - \nu\sigma_{yy}\right)$$
$$\varepsilon_{yy} = \frac{1}{E}\left(\sigma_{yy} - \nu\sigma_{xx}\right) \quad \dots\dots\dots (3)$$

and also proceeding from the assumed-Airy's-stress-function relations

$$\sigma_{xx} = \frac{\partial^2 \Omega}{\partial y^2}$$
$$\sigma_{yy} = \frac{\partial^2 \Omega}{\partial x^2} \quad \dots\dots\dots\dots (4)$$
$$\tau_{xy} = -\frac{\partial^2 \Omega}{\partial x \partial y}$$

we can arrive at the following bi-potential equation

$$\nabla^2(\nabla^2 \Omega) = 0 \quad \dots\dots\dots (5)$$

which can be solved by elaborating the complex-variable technique, the mean normal stress

$$2\bar{\sigma} = \sigma_{xx} + \sigma_{yy} = \nabla^2 \Omega \quad \dots\dots\dots (6)$$

is assumed to be the real part of the analytic function

$$\Theta(z) = \bar{\sigma} + iIm\big(\Theta(z)\big) \quad \dots\dots\dots (7)$$

where $Im\big(\Theta(z)\big)$ is the harmonic conjugate of $\bar{\sigma}$. The integration of $\Theta(z)$ produces another analytic function

$$\Phi(z) = \int \Theta(z) dz \quad \dots\dots (8)$$

Following what had been done by Muskhelishvili **[13]** the following expression, which is consisted of two independent analytic functions, is regarded as the general solution of the Airy's stress function

$$\Omega = \frac{1}{2} Re[\bar{z}\Phi(z) + \Psi(z)] \quad \dots\dots\dots (9)$$

where $\Psi(z)$ is an arbitrarily-introduced analytic function, the derivatives of Ω with respect to x and/or y may give

$$\sigma_{xx} = \frac{\partial^2 \Omega}{\partial y^2} = Re\left(\overline{\Phi} - \frac{\bar{z}\overline{\Phi} + \overline{\Psi}}{2}\right)$$
$$\sigma_{yy} = \frac{\partial^2 \Omega}{\partial x^2} = \left(\overline{\Phi} + \frac{\bar{z}\overline{\Phi} + \overline{\Psi}}{2}\right) \quad \dots\dots\dots (10)$$
$$\tau_{xy} = -\frac{\partial^2 \Omega}{\partial x \partial y} = Im\left(\frac{\bar{z}\overline{\Phi} + \overline{\Psi}}{2}\right)$$

In order to arrive at the displacements, we must invoke the peculiarities of linearly-isotropic-material characteristics (Hooke's law) and the small-strain-theory-based kinematic constraints to (neglecting rigid-body terms emanated due to the translation and/or rotation of the rigid body) proceed into

$$u_x = \frac{1}{4G} Re\left(\left(\frac{3-\nu}{1+\nu}\right)\Phi - \bar{z}\overline{\Phi} - \overline{\Psi}\right)$$
$$u_y = \frac{1}{4G} Im\left(\left(\frac{3-\nu}{1+\nu}\right)\Phi + \bar{z}\overline{\Phi} + \overline{\Psi}\right) \quad \dots\dots (11)$$

Westergaard **[4]** has figured out a relation between the two analytic functions $\Phi(z)$ and $\Psi(z)$ by imposing the boundary condition $\tau_{xy} = 0$ along $y = 0$, for cracks experiencing tension tractions (mode I cracking), so as to proceed into

$$\overline{\Psi} = -z\overline{\Phi} \quad \dots\dots\dots (12)$$

which may be substituted into eq. (10) and into eq. (11) in order to arrive at the following representation for predominant-mode I stresses and displacements

$$\begin{aligned}\sigma_{xx} &= Re\bar{\Phi} - yIm\bar{\bar{\Phi}}\\ \sigma_{yy} &= Re\bar{\Phi} + yIm\bar{\bar{\Phi}} \quad \dots\dots\dots\dots(13)\\ \tau_{xy} &= -yRe\bar{\bar{\Phi}}\end{aligned}$$

$$\begin{aligned}u_x &= \frac{1}{2G(1+\nu)}Re\Phi - yIm\bar{\Phi}\\ u_y &= \frac{1}{G(1+\nu)}Im\Phi - yRe\bar{\Phi}\end{aligned} \quad \dots\dots\dots\dots(14)$$

By firstly solving for stresses and displacements in the vicinity of the crack tip (which lies at $x = a_{cr},\ y = 0$) without any presence of traction stresses, and then imposing the traction stresses at $|x| < a_{cr},\ y = 0$ in order to simulate the crack, Sedov **[9]** has pointed out a general solution for the analytic function $\Phi(z)$ concerning an infinite plate whose crack is having a length of $2a_{cr}$ (Fig. (1)), therefore, we have

$$\bar{\Phi}_I = \frac{1}{\pi\sqrt{z^2 - {a_{cr}}^2}}\int_{-a_{cr}}^{a_{cr}} \frac{\lambda_2(\xi)\sqrt{{a_{cr}}^2 - \xi^2}}{z-\xi}d\xi \dots(15)$$

Introducing the expression for the elastic stress intensity factor

$$K_I = \frac{1}{\sqrt{\pi a_{cr}}}\int_{-a_{cr}}^{a_{cr}} \lambda_2(\xi)\sqrt{\frac{a_{cr}+\xi}{a_{cr}-\xi}}d\xi \quad \dots\dots(16)$$

and studying the behavior of stresses and strains in the vicinity of the right-hand crack tip, ($z + a_{cr} \approx 2a_{cr},\ z - \xi \approx a_{cr} - \xi$), we obtain

$$\bar{\Phi}_I = \frac{K_I}{\sqrt{2\pi(z-a_{cr})}} \quad \dots\dots\dots(17)$$

The introduction of notation ($z - a_{cr} = re^{i\theta}$) and the substitution of eq. (17) into eq.'s (13) and (14) will yield the following local-elastic stress and displacement fields for mode I induced within a purely elastic material

$$\begin{bmatrix}\sigma_{xx}\\ \sigma_{yy}\\ \tau_{xy}\end{bmatrix} = \frac{K_I}{\sqrt{2\pi r}}\cos\frac{\theta}{2}\begin{bmatrix}1-\sin{}^{\theta}\!/_{2}\sin{}^{3\theta}\!/_{2}\\ 1+\sin{}^{\theta}\!/_{2}\sin{}^{3\theta}\!/_{2}\\ \sin{}^{\theta}\!/_{2}\cos{}^{3\theta}\!/_{2}\end{bmatrix} \dots(18)$$

$$\begin{bmatrix}u_x\\ u_y\end{bmatrix} = \frac{K_I}{2G}\sqrt{\frac{r}{2\pi}}\left(\frac{3-\nu}{1+\nu} - \cos\theta\right)\begin{bmatrix}\cos{}^{\theta}\!/_{2}\\ \sin{}^{\theta}\!/_{2}\end{bmatrix} \dots(19)$$

Within the present research elastoplastically-deformed aluminum alloys are to be dealt with, and the Dugdale-assumed elastoplastic intensity factors must therefore be put into consideration instead of the elastic intensity factors. Dugdale analytically proposed that by introducing the traction $\sigma_{yy} = 0$ along $|x| < a_{cr} + c$ and superimposing the traction $\sigma_{yy} = \sigma_Y$ along $a_{cr} < |x| < a_{cr} + c$ (by utilizing the superposition principle) will yield the elastoplastic intensity factor for Tresca-based linear elastic-ideally plastic materials and/or alloys **[2]**

$$K_{I,ep} = \sigma_Y \left[\sqrt{\pi(a_{cr}+c)} - 2\sqrt{\frac{a_{cr}+c}{\pi}} \sin^{-1}\left(\frac{a_{cr}}{a_{cr}+c}\right) \right]$$

$$= \sigma_Y \left[\sqrt{\pi\left(\frac{a_o}{2}+c\right)} - 2\sqrt{\frac{\frac{a_o}{2}+c}{\pi}} \sin^{-1}\left(\frac{\frac{a_o}{2}}{\frac{a_o}{2}+c}\right) \right] \dots (20)$$

where σ_Y is the yield stress whose values must be determined by invoking the peculiarities of the plate theory, which is to be discussed within the upcoming article, in conjunction with the Tresca's failure criterion. c is the plastic zone size, which is emanated from the crack tip, whose values are to be determined by following what had been done by Dugdale **[2]** in order to arrive at

$$c = \frac{\pi}{8}\left(\frac{K_I}{\sigma_Y}\right)^2 = \frac{a_o}{16}\left(\frac{\pi\sigma_y}{\sigma_Y}\right)^2 \dots\dots\dots\dots (21)$$

Now, it is meaningfully convenient to proceed into the following elastoplastic-crack-tip-nearby stress, displacement, and strain fields

$$\begin{bmatrix} \sigma_{xx} \\ \sigma_{yy} \\ \tau_{xy} \end{bmatrix}_{ep} = \frac{K_{I,ep}}{\sqrt{2\pi r}} \cos\frac{\theta}{2} \begin{bmatrix} 1 - \sin\theta/2 \sin 3\theta/2 \\ 1 + \sin\theta/2 \sin 3\theta/2 \\ \sin\theta/2 \cos 3\theta/2 \end{bmatrix} \dots (22)$$

$$\begin{bmatrix} u_x \\ u_y \end{bmatrix}_{ep} = \frac{K_{I,ep}}{2G}\sqrt{\frac{r}{2\pi}}\left(\frac{3-\nu}{1+\nu} - \cos\theta\right) \begin{bmatrix} \cos\theta/2 \\ \sin\theta/2 \end{bmatrix} (23)$$

$$\begin{bmatrix} \varepsilon_{xx} \\ \varepsilon_{yy} \\ \gamma_{xy} \end{bmatrix}_{ep} = \begin{bmatrix} \frac{\Delta u_{x,ep}}{\Delta x} \\ \frac{\Delta u_{y,ep}}{\Delta y} \\ \frac{\Delta u_{x,ep}}{\Delta y} + \frac{\Delta u_{y,ep}}{\Delta x} \end{bmatrix} \dots\dots\dots (24)$$

2.2 The Plate Theory and Tresca's Failure Criterion:

The general equation that governs the deflection of a simply-supported rectangular plate, which has a length b, width a, and thickness h, is always represented by a double trigonometric series, therefore, we have **[18]**

$$w = \frac{-4F(t)}{\pi^4 abD} \sum_{m=1}^{\infty}\sum_{n=1}^{\infty} \left[\frac{\sin\left(\frac{m\pi\xi}{a}\right)\sin\left(\frac{n\pi\eta}{b}\right)}{\left(\frac{m^2}{a^2}+\frac{n^2}{b^2}\right)^2} \right] * \sin\left(\frac{m\pi x}{a}\right)\sin\left(\frac{n\pi y}{b}\right) \dots (25)$$

Since the bending moments about x and y axes depend upon the 2nd derivatives of the deflection equation with respect to x and y as shown below

$$\begin{bmatrix} M_x \\ \\ M_y \end{bmatrix} = \frac{4F(t)}{\pi^4 ab} \sum_{m=1}^{\infty} \sum_{n=1}^{\infty} \begin{bmatrix} \left(\frac{m^2}{a^2} + \nu \frac{n^2}{b^2}\right) \\ \left(\frac{n^2}{b^2} + \nu \frac{m^2}{a^2}\right) \end{bmatrix} * \frac{\sin\left(\frac{m\pi\xi}{a}\right) \sin\left(\frac{n\pi\eta}{b}\right) \sin\left(\frac{m\pi x}{a}\right) \sin\left(\frac{n\pi y}{b}\right)}{\left(\frac{m^2}{a^2} + \frac{n^2}{b^2}\right)^2} \dots (26)$$

where $F(t)$ is the time-dependent impacting force which strikes the thin plate in a very short-time duration (by utilizing a pistol of a Glock-18 model whose bullet's specifications are given in table (1)) and it is engineered to deform the thin plate elastoplastically, further data for the aluminum-alloys specifications are illustrated in table (2). To acquire the full-configuration-short-time-duration impacting load, it is adequately convenient to utilize the principles of work and energy (neglecting the air-resistance effects and temperature-change energy losses) and linear momentum principles as well as the triangular-type-impact-load assumption. We can therefore arrive at the short-time-duration impacting force **[15]**

$$F(t) = P_o A_o \left(1 - \frac{(P_o A_o)t}{2m_o\sqrt{v_1^2 + gd}}\right) \dots (27)$$

Since the bending moments can be proceeded into the in-plane elastic stresses **[18]**

$$\begin{bmatrix} \sigma_{xx} \\ \sigma_{yy} \\ \tau_{xy} \end{bmatrix} = \frac{1}{h^2} \begin{bmatrix} 6M_x \\ 6M_y \\ 3M_x \end{bmatrix} \dots\dots\dots\dots (28)$$

and consequently to the plane-stress-based elastic principal stress

$$\begin{bmatrix} \sigma_1 \\ \\ \sigma_2 \end{bmatrix} = \begin{bmatrix} \frac{\sigma_x + \sigma_y}{2} + \sqrt{\left(\frac{\sigma_x - \sigma_y}{2}\right)^2 + (\tau_{xy})^2} \\ \frac{\sigma_x + \sigma_y}{2} - \sqrt{\left(\frac{\sigma_x - \sigma_y}{2}\right)^2 + (\tau_{xy})^2} \end{bmatrix} \dots (30)$$

in which $\sigma_3 = 0$ for the plane-stress state, it is meaningful to finally arrive at the Dugdale-proposed predominant-yield-stress value by using Tresca's criterion **[19]**

$$\sigma_Y = \sigma_1 - \sigma_3 = \sigma_1 \dots\dots\dots (31)$$

Glock-18-Bullet Specifications **[8][14]**	
Muzzle velocity (v_1)	$375\ {}^{m}/_{s}$
Bullet Mass(m_o)	$0.00745\ kg$
Bullet Type Used	$9 * 19mm\ Parabellum$
Rated Maximum Striking Pressure of a Bullet (P_o)	$500\ Mpa$
Distance between the Pistol and the Thin Plate (d)	$0.45\ m$
Contact Area between the Bullet and the Thin Plate (A_o)	$\frac{\pi}{4} * 9^2\ mm^2$

Table (1) Impacting-Bullets Specifications

Pure Aluminum 1100 Properties **[11]**	
Poisson's Ratio (ν)	0.334
Young's Modulus (E)	69 Gpa
Shear Modulus (G)	26 Gpa
Yield Limit (YS)	8 Mpa
Specific Density (ρ)	2720 $^{kg}/_{m^3}$
Aluminum Copper 2014 Properties **[6]**	
Poisson's Ratio (ν)	0.330
Young's Modulus (E)	72 Gpa
Yield Limit (YS)	11 Mpa
Specific Density (ρ)	2800 $^{kg}/_{m^3}$

Table (2) Aluminum-Alloys Specifications

2.3 Crack Development: Criteria and Analyses:

The Griffith crack criterion states: a crack grows to a further size if the energy required to from an additional crack da_{cr} can just be delivered by a system. It has been demonstrated that at the onset of fracture instability the energy release rate (which is equal to $\frac{{K_I}^2}{E}$ for the plane-stress-based-opening-mode cracking **[1]**) given by

$$G_I = \frac{d}{da_{cr}}(F_e - U_e) \dots\dots\dots (32)$$

where F_e is the external-load work and U_e is the plate elastic energy, is equal to the crack resistance (which equals the critical energy release rate $G_{Ic} = \frac{\pi a_c {\sigma_\infty}^2}{E}$ at the fracture-instability onset) given by

$$R = \frac{dW_{cr}}{da_{cr}} \dots\dots\dots\dots (33)$$

where W_{cr} is the crack-formation energy. A total analysis should therefore lead to the fact that the energy release rate is the same as the critical one at the onset of instability, therefore, we obtain

$$G_I = G_{Ic} \leftrightarrow \frac{{K_I}^2}{E} = \frac{\pi a_c {\sigma_\infty}^2}{E} \leftrightarrow a_c = \frac{1}{\pi}\left(\frac{K_I}{\sigma_y}\right)^2 \dots (34)$$

for purely elastic materials like glass, for elastoplastically-deformed alloys we utilize

$$a_c = \frac{1}{\pi}\left(\frac{K_{I,ep}}{\sigma_y}\right)^2 \dots\dots\dots\dots\dots (35)$$

The crack-size critical value a_c is regarded as the illustrating value of whether or not the crack is propagating, and a hypothesis should therefore be kept in consideration in order to recognize the crack-development state

- The crack cannot grow to any further size when the existing crack size within the impacted plate is less than the critical-crack-size value, i.e., $a_{cr} < a_c$.
- The crack will propagate and immediately stop only when the existing crack size is just approaching the critical-crack-size value, i.e., $a_{cr} \approx a_c$.

- Dynamic crack propagation will occur and the crack will grow continuously when the impacted-plate-existed crack size is larger than the critical crack size, i.e., $a_{cr} > a_c$, moreover, the kinetic-energy-based crack propagation speed (suggested by Mott **[12]**) is therefore given by

$$\dot{a}_{cr} \approx 0.38\sqrt{\frac{E}{\rho}}\left(1-\frac{a_c}{a_{cr}}\right) \approx 0.38\sqrt{\frac{E}{\rho}}\left(1-\frac{2a_c}{a_o}\right) \dots\dots (36)$$

3. Experimental Technique:

3.1 Cracks-and-Grids-Implementation Process:

Once the initially-existed-flaws testing, surface-finish testing, and chemical-composition testing for the 6mm-thickness-aluminum-alloy specimens, whose specifications are illustrated in table (3), are accomplished (Fig. (2) to Fig. (4)), grids and cracks are engraved within the aluminum-alloy-based plates surface using a computer-controlled CNC machine (Fig. (5)) **[20]**. Table (4) is underlining the specifications for the implemented cracks and grids within the surface of pure aluminum 1100 and aluminum copper 2014 plates.

Type	No.	Dimensions	Aspect Ratio	Crack Length
Pure Aluminum 1100	3	21*21cm	1.0000	1cm, 2cm, and 3cm
Pure Aluminum 1100	3	21*16cm	1.3334	1cm, 2cm, and 3cm
Pure Aluminum 1100	3	21*11cm	2.0000	1cm, 2cm, and 3cm
Aluminum-Copper 2014	3	21*21cm	1.0000	1cm, 2cm, and 3cm
Aluminum-Copper 2014	3	21*16cm	1.3334	1cm, 2cm, and 3cm
Aluminum-Copper 2014	3	21*11cm	2.0000	1cm, 2cm, and 3cm

Table (3) Aluminum-Alloy Plates Specifications

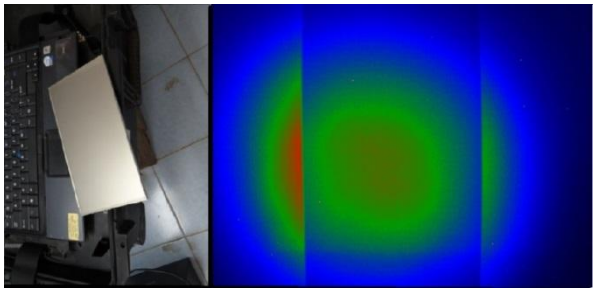

Fig. (2) The Initially-Existed-Flaws X-ray Testing for the Aluminum-Alloy Plates. All Plates are Exhibiting Good Surface Properties

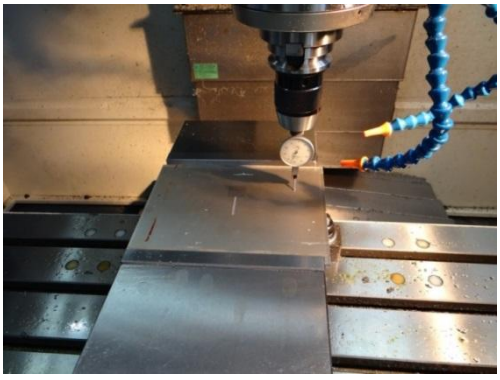

Fig. (3) Aluminum-Alloy Plates Surface-Finish Testing

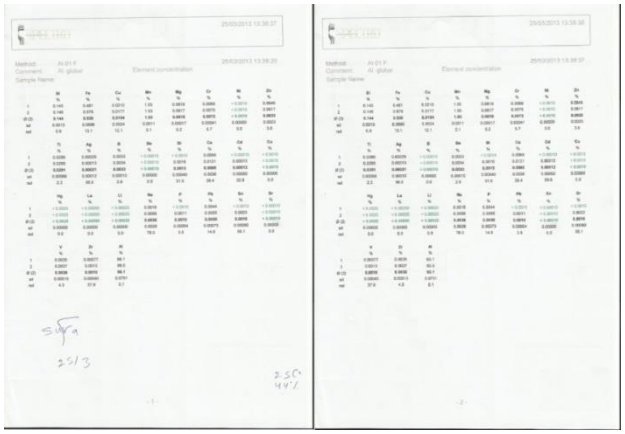

Fig. (4) Plates Chemical-Composition Testing. The Left and the Right Pictures Exhibit the Element-Concentrations List for Pure Aluminum 1100 and Aluminum Copper 2014 Specimens, Respectively.

Fig. (5) The Crack-and-Grid-Implementing Computer-Controlled CNC Machine.

Grid Specifications	
Dimensions	$20mm * 20mm$
Spacing Between Each Grid Line	$1mm$
Depth of the Grid Line	$0.001mm$
Width of the Grid Line	$0.1mm$
Crack Specifications	
Crack Type	Surface Crack
Crack Position	Centered Crack
Crack Depth	$2mm$

Table (4) The-Engraved-Cracks-and-Grids Specifications.

3.2 The-Impact-Testing Unit:

The test unit shown in Fig. (6) is to be executing the impact test for all the aluminum-alloy plates **[3]**. To hold the whole testing unit in place, connecting bolts engraved into the ground are fixing the test rig without being displaced nor rotated in any direction during the-impact-test occurrence. Supports on which the specimens are to be mounted are found within the internal frame of the test unit, these three supports are dimensioned in such a way that all the plate are, with an accurate way of establishing the plates onto the corresponding supports and these plates are then connected with the internal frame by 6mm-diameter connecting bolts, mounted onto their corresponding supports (Fig. (7)). The test-unit external frame contains a rectangular thick plate, made from wood and used to fit perfectly with the external frame (Fig.

(6)), which is having three holes through which the bullets, launched by a Glock-18-type sidearm, are striking the thin plates mounted on the within-the-internal-frame supports. These holes are engineered so that, since the pistol's end is to coincide perfectly with the designed hole, the pistol is accurately directed towards the grid-nearby-right-hand-crack-tip where the crack is expected to traverse through the continuum considered. Finally, the four faces forming the surface area of the test unit are covered by steel sheets, riveted altogether with the test-unit external structure, in order to avoid any inconvenient hazards which may be resulted from the-striking-bullets rebound or from the launched-bullets harmful temperature.

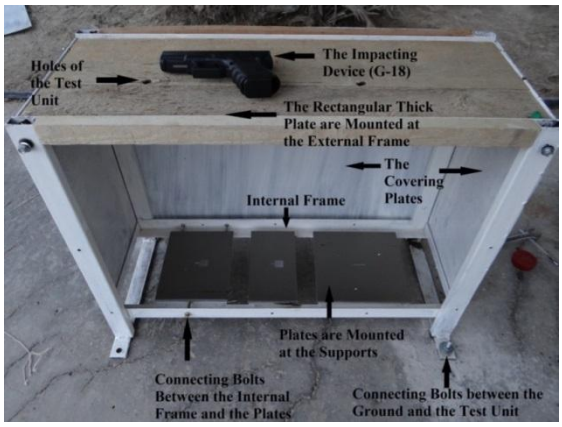

Fig. (6) The-Impact-Testing Unit

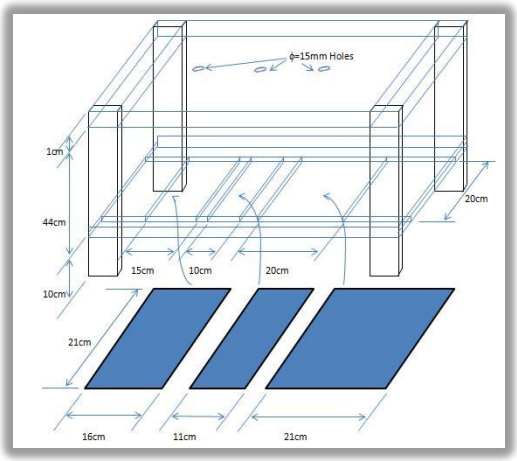

Fig. (7)The-Test-Unit Dimensions Needed to Execute the Impact Process

3.3 Aluminum-Plates Microstructure-Testing Unit:

In order to arrive at the permanently-induced displacements, plastic-zone extents, and dynamically-propagating-cracks speeds, a computer-controlled microscope is processed to arrive at the experimental output data before and after the impact-process occurrence **[5]**. As shown in Fig. (8), the computer-controlled microstructure-testing unit is elaborated so as to proceed into the grid configuration before and after the-impact-test achievement. The experimental technique can therefore be summarized into the following overall procedure in Fig. (9) shown below.

Fig. (8) The-Computer-Controlled Microstructure-Testing Unit

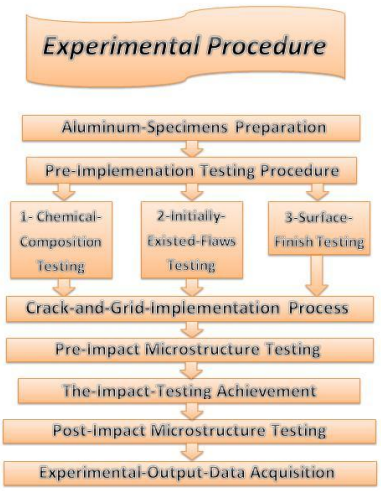

Fig. (9) The Experimental-Technique Procedure

4. Results and Discussion:

4.1 Plastic-Zone Size:

Referring to Fig (10), it is found that the plastic-zone extent increases as the crack length increases, and it is also found that the more the plate aspect ratio is, the less the plastic-zone extent will be. A further illustration must therefore lead to the fact that the pure aluminum1100 plates are exhibiting more yielded-zone extents than what is exhibited by the aluminum copper 2014 ones.

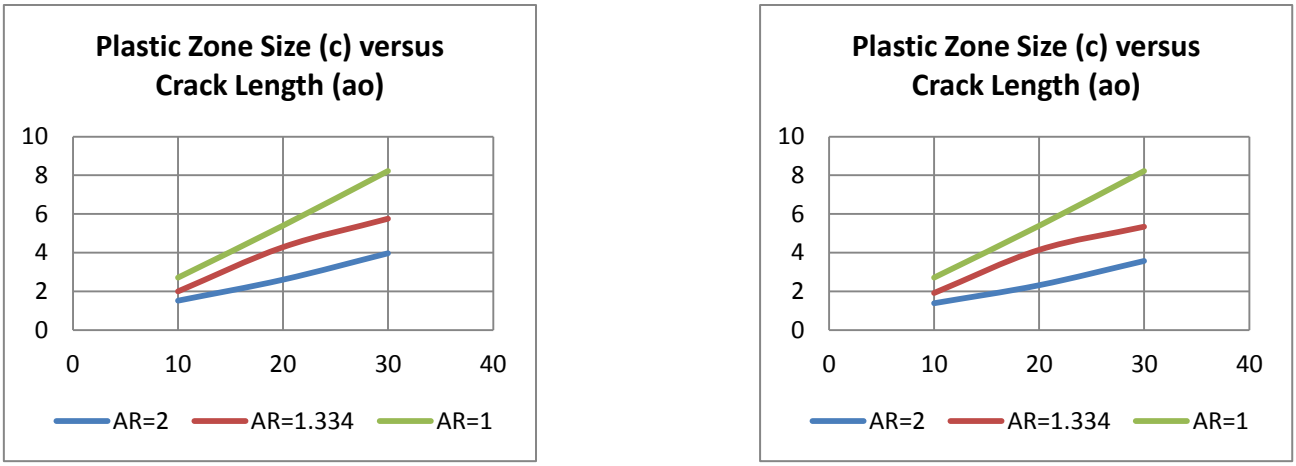

Fig. (10) The Plastic-Zone Size. The Left and The Right Charts are for Pure Aluminum 1100 and Aluminum Copper 2014 Plates Respectively.

4.2 Crack-Development Speed:

It has been previously shown that the critical crack length is the decisive value to illustrate whether or not the crack is propagating, it is demonstrated theoretically and experimentally that the crack will dynamically propagate through a certain path within the aluminum-alloy plates. Fig (11) is indicating that the crack-development speed decreases as the crack length increases **[10]**, and also is implying that the high-aspect-ratio plates experience higher propagating-cracks speeds than the low-aspect-ratio plates. Moreover, the pure aluminum 1100 plates are exhibiting less propagating-cracks-speeds than the aluminum copper 2014 ones.

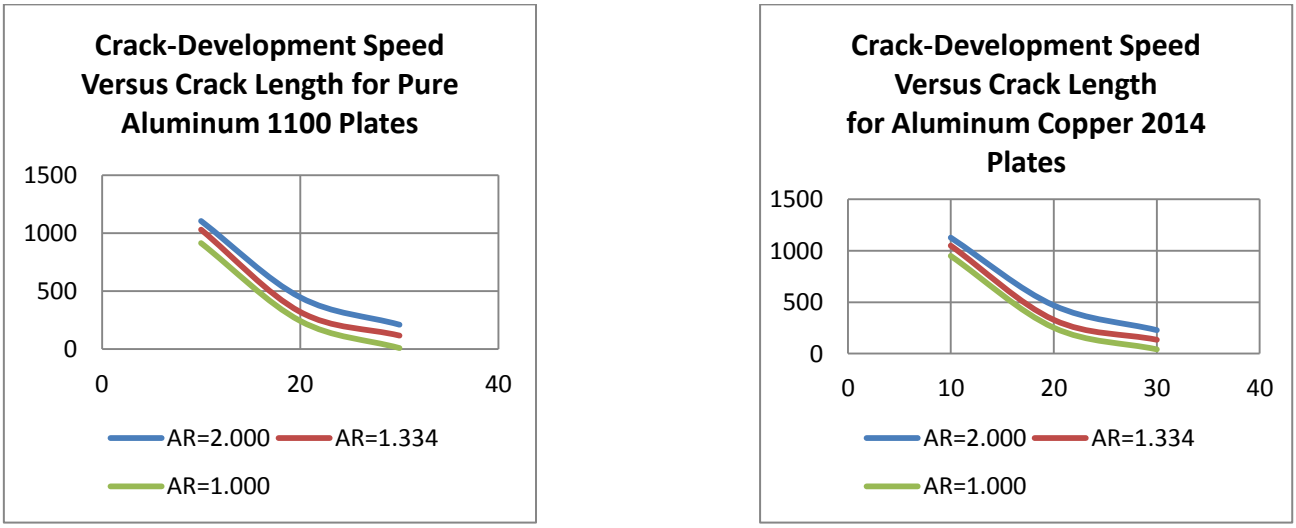

Fig. (11) The Crack-Development Speed. The Left and The Right Charts are for Pure Aluminum 1100 and Aluminum Copper 2014 Plates Respectively.

4.3 Crack-Tip-nearby-Stress Field:

It is demonstrated, referring to Fig. (12) for 10-mm-crack-length and 1-aspect-ratio pure aluminum 1100 plate, that the more the distance of the gridpoint from the crack tip is, the less the stresses within that gridpoint will be. The elastoplastic stresses attain their maximum values at the instant when the impacting bullet is just striking the thin plate, i.e. $t = 0$.

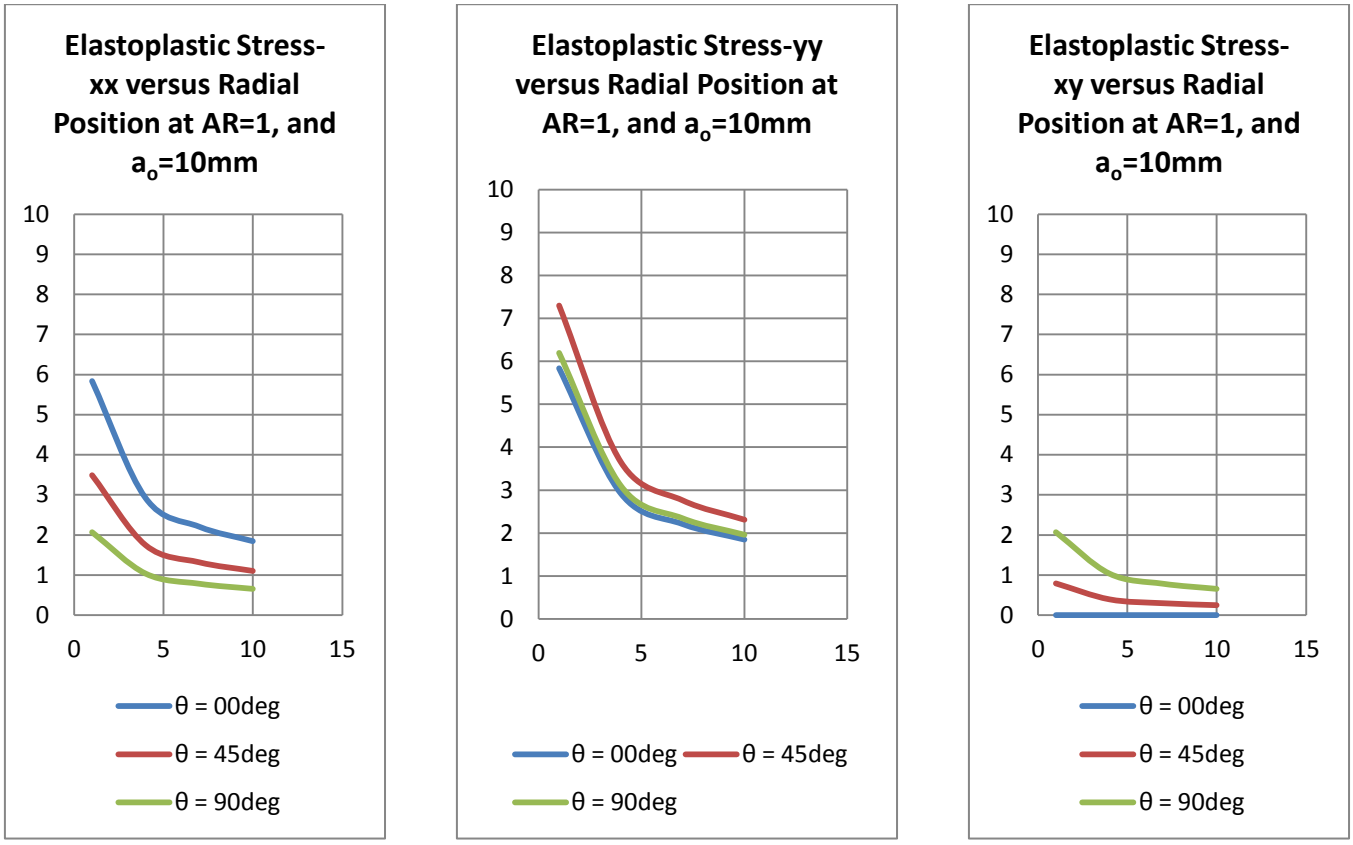

Fig. (12) Crack-Tip-nearby Elastoplastic Stress Field

4.4 Experimental Crack-Tip-nearby-Strain Field:

It is concluded experimentally, with the aid of Fig. (13), that the crack-tip-nearby-strain field values are increasing as the distance between the gridpoints and the crack tip decreases, until these strain values attain their maximum values at the point where the crack tip lies at. The upcoming charts, found within Fig. (13), are elaborated to establish the strain-field behavior for a pure aluminum 1100 plate whose crack length and aspect ratio are 10mm and 1, respectively.

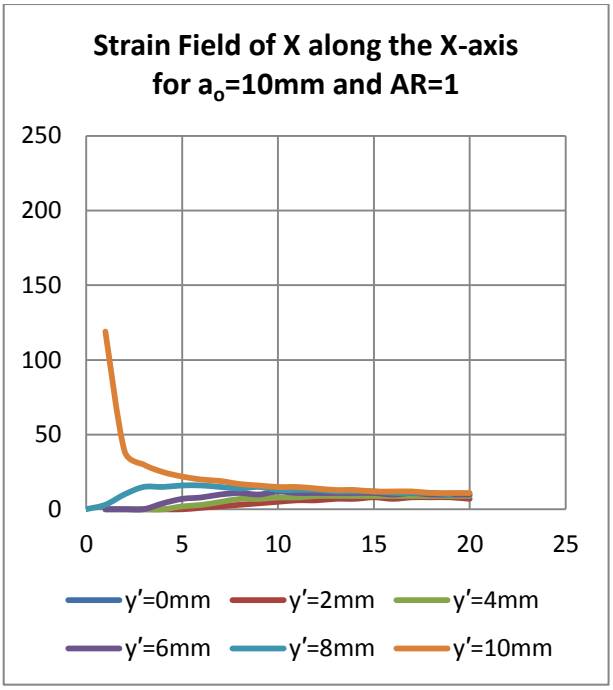

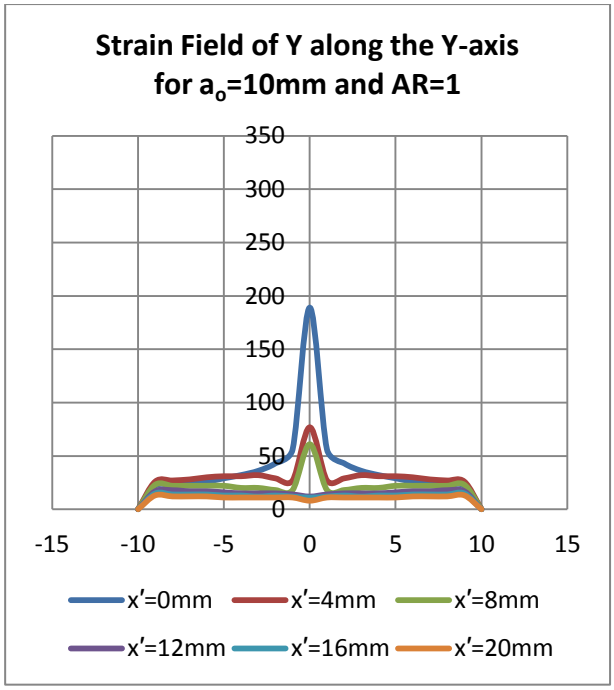

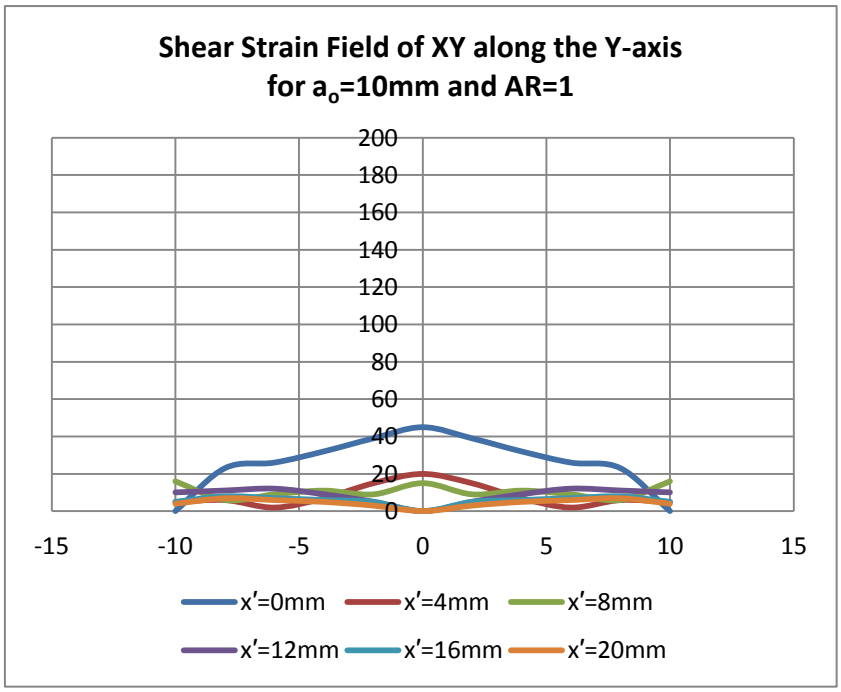

Fig. (13) Crack-Tip-nearby Strain Field.

5. Concluding Remarks:

The Discussed analytical and experimental results demonstrate the fact that whichever increase is encountered to the yielded-zone-size values, which is resulted from the long-cracks utilization or plate-aspect-ratio reduction, etc., leads to some decrease in the crack-development-speed values for an elastoplastically-deformed cracked plate, and vice versa. Furthermore, a total analysis should therefore proceed into the establishment of the crack-tip-nearby elastoplastic stress and strain fields' behavior, and also lead to the required satisfactory-design environment thereafter.

Acknowledgments:

Special thanks are given to my father Abdul-Hussein Ali Owayez, to my mother Hussniyah Alwan Maseer, and to my co-author Fathy Abdul-Sahib Al-Shamma for their unending and valuable efforts.

Appendices:

Appendix (1): The Analytical-Technique-Based-Flow-Chart:

All the analytic-solution-based expressions for the continuum considered are already dealt with, in order to illustrate the effect of the parameters studied. The Analytical Solution should therefore requires obeying the upcoming flow chart

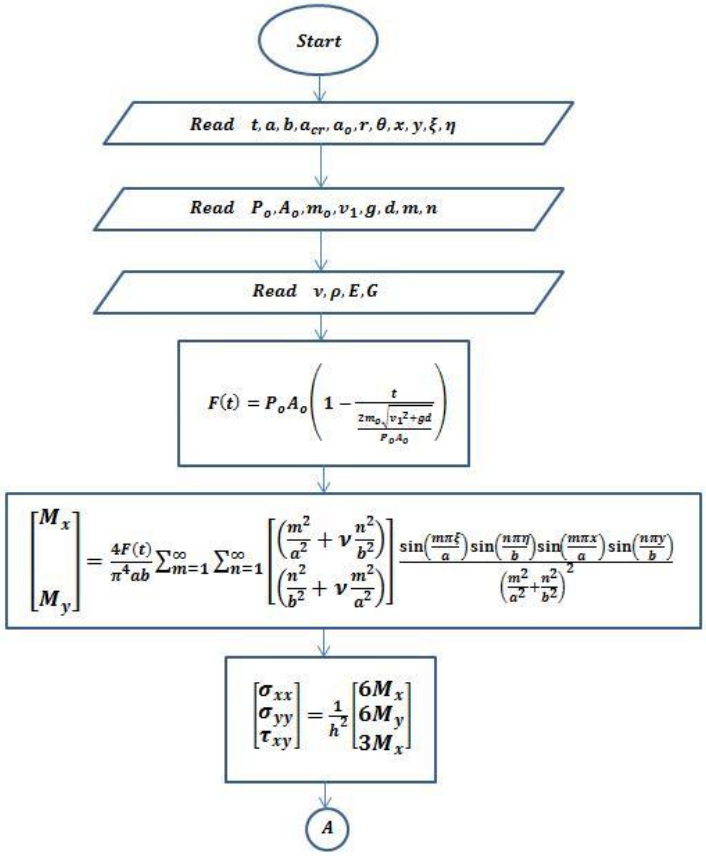

Fig. (A1) The Analytical-Solution-Based Flow Chart

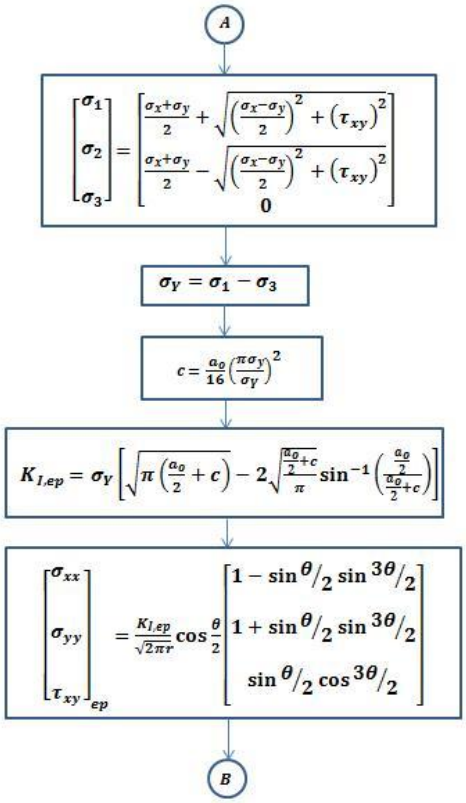

Fig. (A2) The Analytical-Solution-Based Flow Chart (Continued)

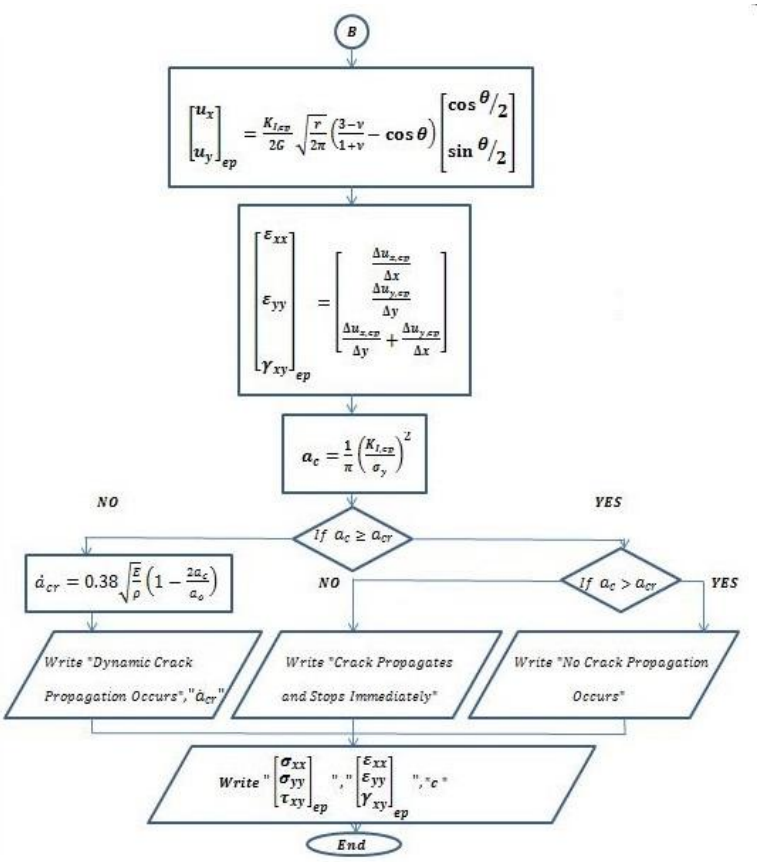

Fig. (A3) The Analytical-Solution-Based Flow Chart (Continued)

Appendix (2): The-Experimental-Output Data:

The Experimental output data, for a pure aluminum 1100 plate whose crack length and aspect ratio are 10mm and 1, respectively, are illustrated in the following table

X(mm)	Y(mm)	U_x(μm)	U_y(μm)
0	0	0	0
4	0	264	0
8	0	373	0
12	0	457	0
16	0	528	0
20	0	590	0
0	2	264	267
4	2	300	71
8	2	387	48
12	2	465	38
16	2	533	33
20	2	594	30
0	4	373	378
4	4	375	157
8	4	425	101
12	4	487	80
16	4	548	68
20	4	605	60
0	6	458	463
4	6	452	245
8	6	475	160
12	6	520	124
16	6	571	104
20	6	622	92
0	8	528	535
4	8	522	326
8	8	530	222
12	8	560	171
16	8	601	143
20	8	645	125
0	10	591	598
4	10	585	400
8	10	586	285
12	10	604	221
16	10	635	184
20	10	672	160
Plastic Zone Size		2.50mm	
Crack Extension		11mm	

Table (A1) The Experimental Output Data for 10mm-Crack-Length and 1-Aspect-Ratio Pure Aluminum 1100 Thin Plate

References:

1. David Broek; "*Elementary Engineering Fracture Mechanics*"; Martinus Nijhoff Publishers; (1982).
2. D. S. Dugdale; "*Yielding of Steel Sheets Containing Slits*"; Journal of the Mechanics and Physics of Solids, Volume 8, Issue 2; PP 100-104; Elsevier; (1960).
3. G.G. Corbett, S. R. Reid, W. Johnson; "*Impact Loading of Plates and Shells by Free-Flying Projectiles: A Review*"; International Journal of Impact Engineering, Volume 18, Issue 2; Elsevier: (1996).
4. H. M. Westergaard; "*Bearing Pressures and Cracks*"; Journal of Applied Mechanics, Volume 61; PP 49-53; (1939).
5. J. H. Underwood, D. P. Kendall; "*Measurement of Microscopic Plastic Strain Distributions in a Region of a Crack Tip*"; Journal of Experimental Mechanics, Volume 9, Issue 7: PP296-304; Springer; (1969)
6. J. Polmear; "*Light Alloys: Metallurgy of Light Metals*", Third Edition; Butterworth Heinmann; (1995).
7. Kare Hellan; "*Introduction to Fracture Mechanics*"; University of Trondheim, Norway; Mc Graw Hill Book Company; (1985).
8. Kevin Dockery; "*Future Weapons*"; Copyrighted Material, New York: Penguin; (2007).
9. L. I. Sedov; "*A Course in Continuum Mechanics*"; Kluwer Academic Publishers; (1972).
10. Marek Krawczuk, Magadalena Palacz, Wieslaw Ostachowicz; "*Wave Propagation in Plate Structures for Crack Detection*"; Journal of Finite Element Design and Analysis, Volume 40; PP 991-1004; Elsevier; (2004).
11. Michael F. Ashby, David R. H. Jones; "*Engineering Materials 1: An Introduction to Their Properties and Applications*", Second Edition; Butterworth Heinmann; (1996).
12. N. F. Mott; "*Fracture of Metals: Some Theoretical Considerations*"; Journal of Engineering, Volume 165; PP 16-18; (1948).
13. N. I. Muskhelishvili; "*Some Basic Problems of the Fundamental Theory of Elasticity*", Second Edition; Kluwer: The Language of Science; (1977).
14. Proof of Ordnance; "*Munitions, Armor and Explosives*"; Ministry of Defence; Standard 05-101; Part 1; (2007).
15. R. C. Hibbeler; "*Engineering Mechanics: Dynamics*"; Pearson, Prentice Hall; (2007).
16. Richard W. Hertzberg; "*Deformation and Fracture Mechanics of Engineering Materials*", Fourth Edition; Materials Research Center, Lehigh University, USA; John Wily and Sons Inc.; (1996).
17. T. Ngo, P. Mendis, A. Gupta, J. Ramsay; "*Blast Loading and Blast Effects on Structures: An Overview*"; Journal of Loading on Structures; EJSE International; (2007).
18. S. P. Timoshenko, S. Woinowsky-Krieger;"*Theory of Plates and Shells*", Second Edition; Mc-Graw Hill International Edition; (1959).
19. W. Johnson, P.B. Mellor; "*Plasticity for Mechanical Engineers*"; Van Nostrand Reinhold Company, London; (1962).
20. Y. C. Leung, L. C. Chan, C. Y. Tang, T. C. Lee; "*An Effective Process of Strain Measurement for Severe and Localized Plastic Deformation*"; International Journal of Machine Tools and Manufacture, Volume 44; PP 669-676; Elsevier; (2004).

Figure

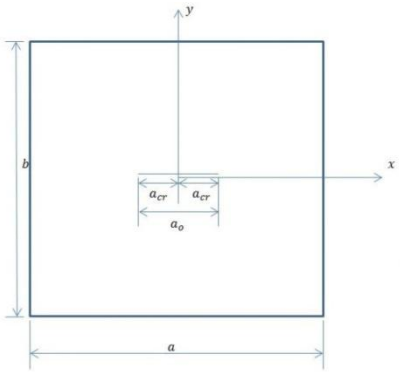

Fig. (1) The Centrally-Cracked-Plate Mathematical Model

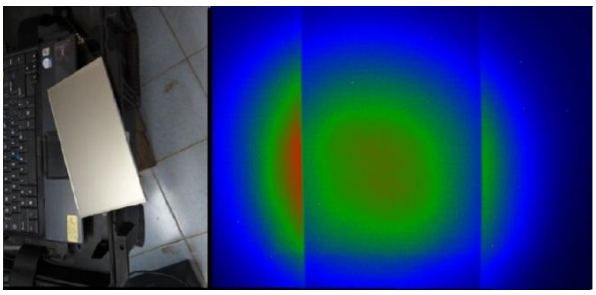

Fig. (2) The Initially-Existed-Flaws X-ray Testing for the Aluminum-Alloy Plates. All Plates are Exhibiting Good Surface Properties

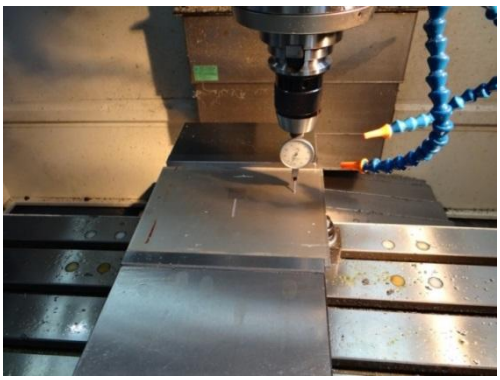

Fig. (3) Aluminum-Alloy Plates Surface-Finish Testing

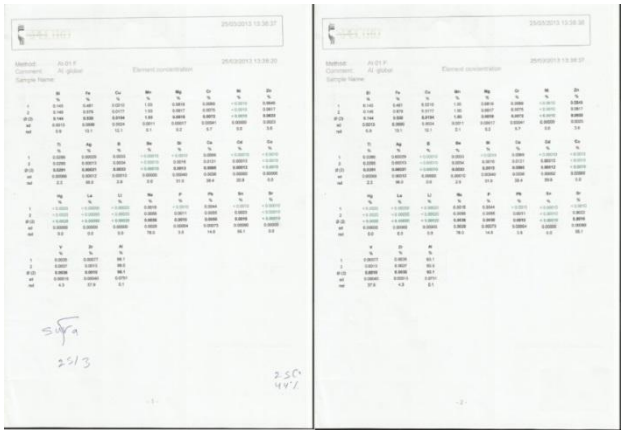

Fig. (4) Plates Chemical-Composition Testing. The Left and the Right Pictures Exhibit the Element-Concentrations List for Pure Aluminum 1100 and Aluminum Copper 2014 Specimens, Respectively.

Fig. (5) The Crack-and-Grid-Implementing Computer-Controlled CNC Machine.

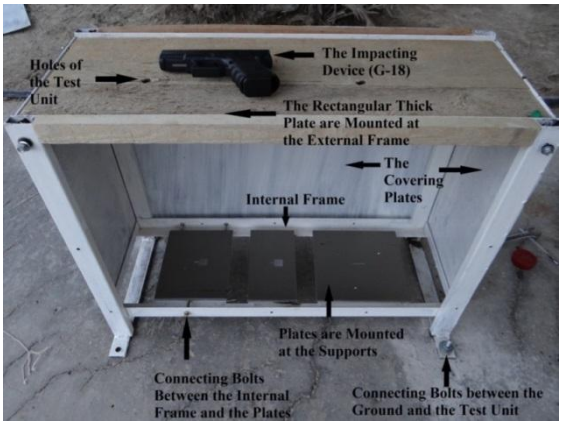

Fig. (6) The-Impact-Testing Unit

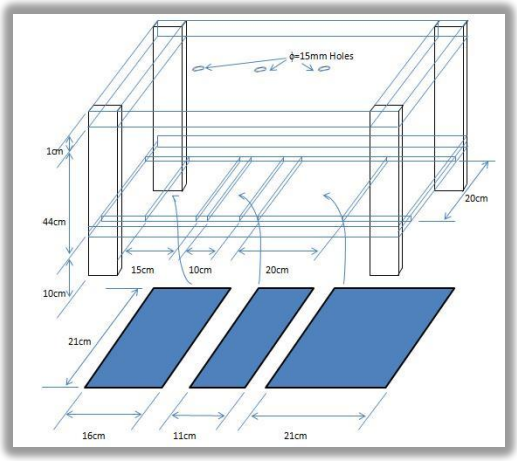

Fig. (7)The-Test-Unit Dimensions Needed to Execute the Impact Process

Fig. (8) The-Computer-Controlled Microstructure-Testing Unit

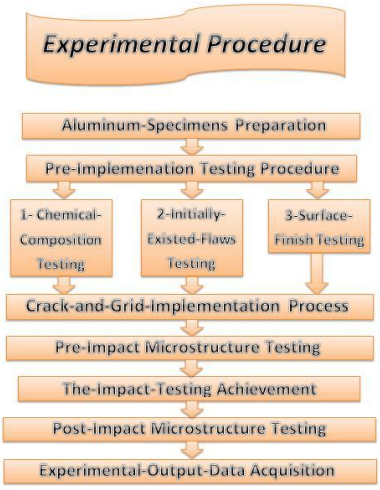

Fig. (9) The Experimental-Technique Procedure

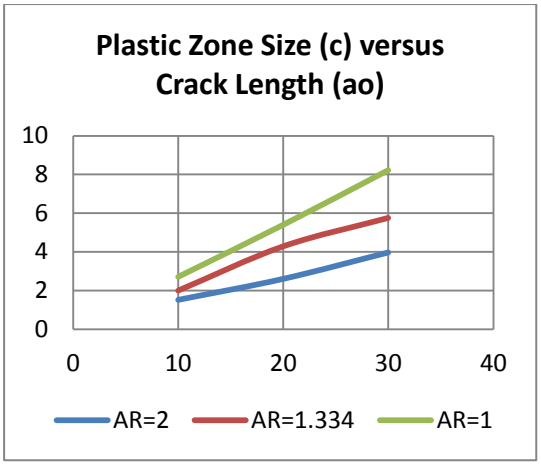

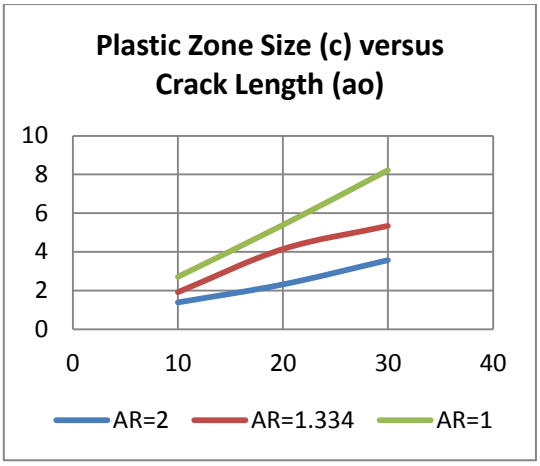

Fig. (10) The Plastic-Zone Size. The Left and The Right Charts are for Pure Aluminum 1100 and Aluminum Copper 2014 Plates Respectively.

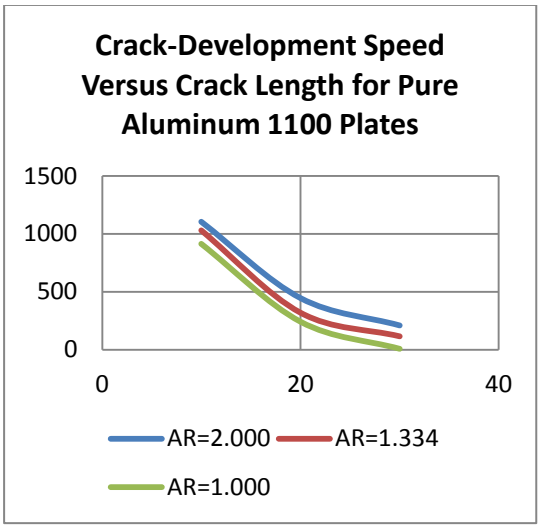

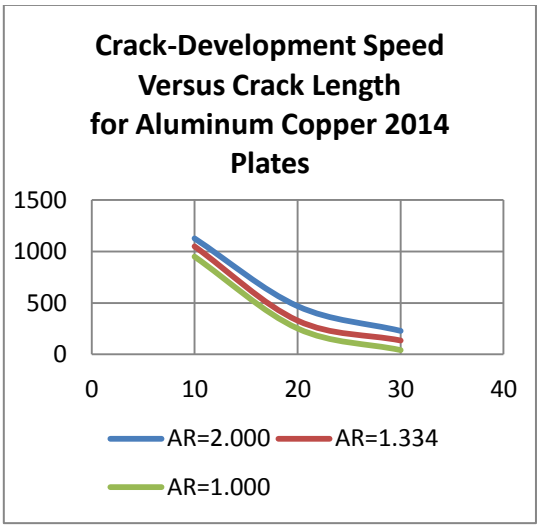

Fig. (11) The Crack-Development Speed. The Left and The Right Charts are for Pure Aluminum 1100 and Aluminum Copper 2014 Plates Respectively.

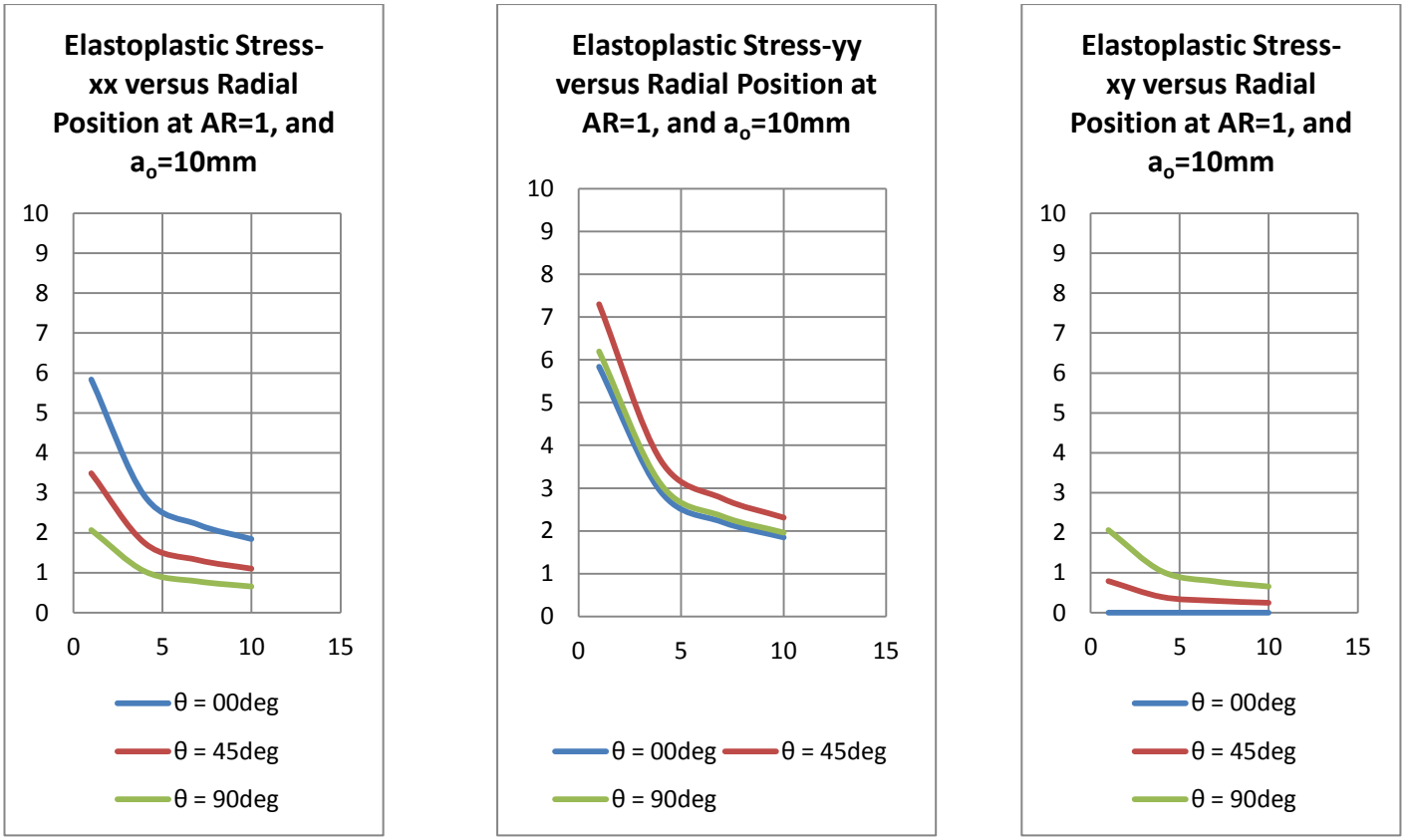

Fig. (12) Crack-Tip-nearby Elastoplastic Stress Field

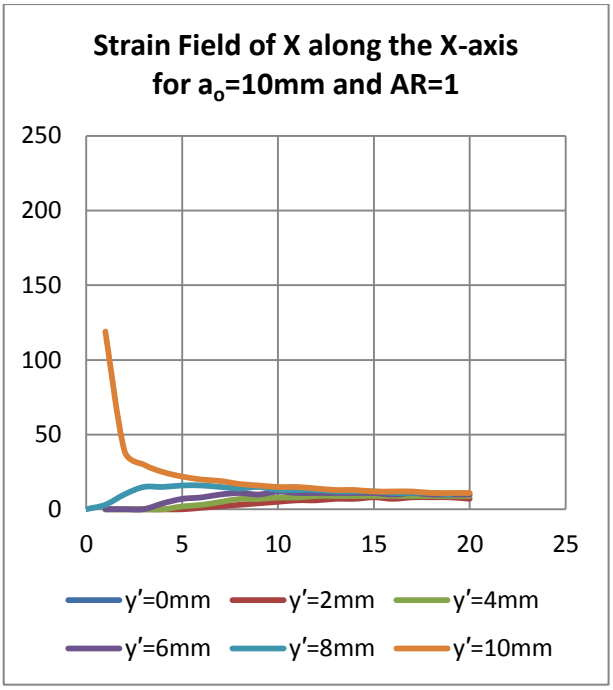

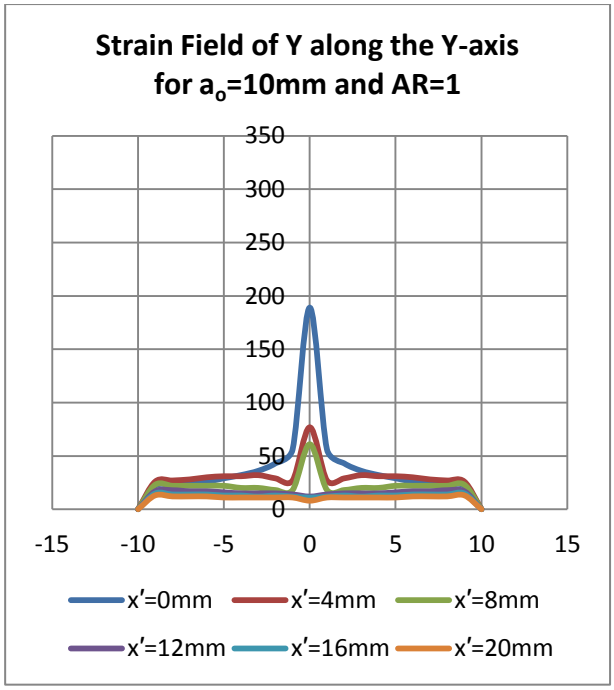

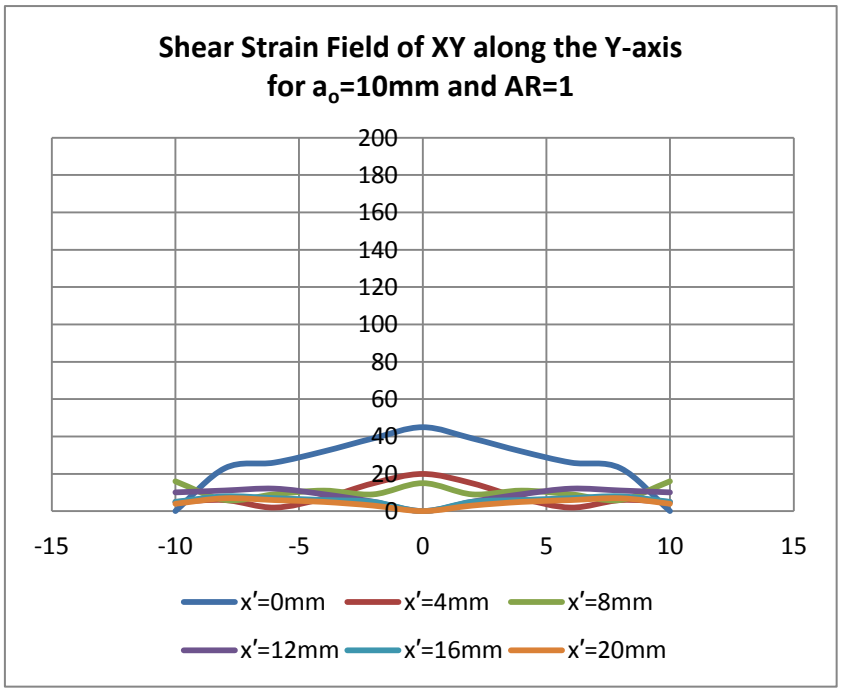

Fig. (13) Crack-Tip-nearby Strain Field.

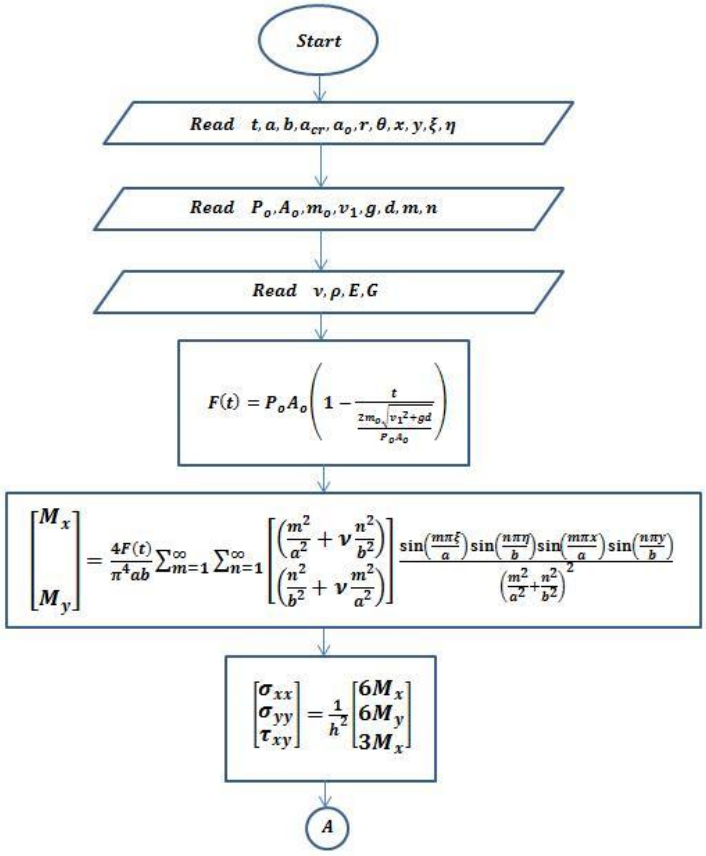

Fig. (A1) The Analytical-Solution-Based Flow Chart

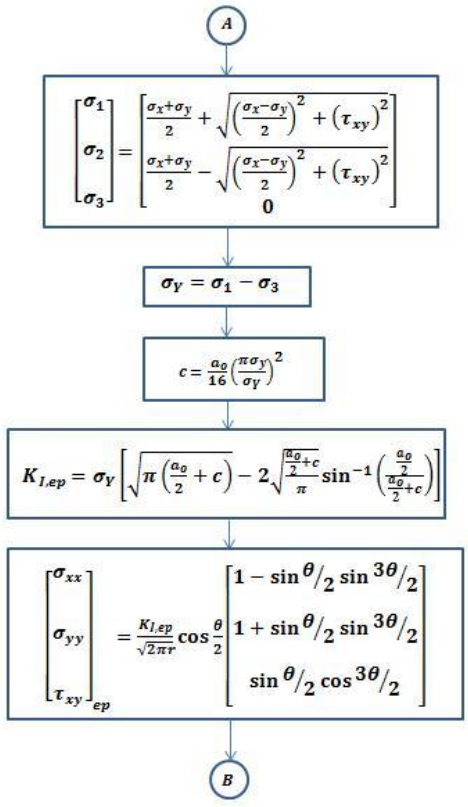

Fig. (A2) The Analytical-Solution-Based Flow Chart (Continued)

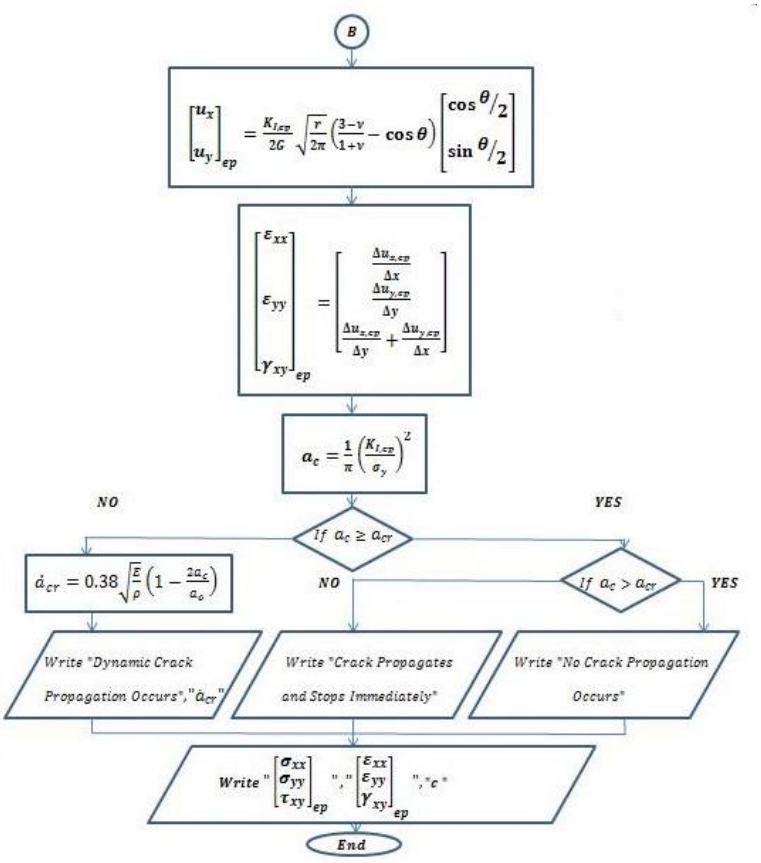

Fig. (A3) The Analytical-Solution-Based Flow Chart (Continued)

Table

Glock-18-Bullet Specifications **[8][14]**	
Muzzle velocity (v_1)	$375\ {}^{m}/_{s}$
Bullet Mass(m_o)	$0.00745\ kg$
Bullet Type Used	$9 * 19mm\ Parabellum$
Rated Maximum Striking Pressure of a Bullet (P_o)	$500\ Mpa$
Distance between the Pistol and the Thin Plate (d)	$0.45\ m$
Contact Area between the Bullet and the Thin Plate (A_o)	$\frac{\pi}{4} * 9^2\ mm^2$

Table (1) Impacting-Bullets Specifications

Pure Aluminum 1100 Properties **[11]**	
Poisson's Ratio (v)	0.334
Young's Modulus (E)	$69\ Gpa$
Shear Modulus (G)	$26\ Gpa$
Yield Limit (YS)	$8\ Mpa$
Specific Density (ρ)	$2720\ {}^{kg}/_{m^3}$
Aluminum Copper 2014 Properties **[6]**	
Poisson's Ratio (v)	0.330
Young's Modulus (E)	$72\ Gpa$
Yield Limit (YS)	$11\ Mpa$
Specific Density (ρ)	$2800\ {}^{kg}/_{m^3}$

Table (2) Aluminum-Alloys Specifications

Type	No.	Dimensions	Aspect Ratio	Crack Length
Pure Aluminum 1100	3	21*21cm	1.0000	1cm, 2cm, and 3cm
Pure Aluminum 1100	3	21*16cm	1.3334	1cm, 2cm, and 3cm
Pure Aluminum 1100	3	21*11cm	2.0000	1cm, 2cm, and 3cm
Aluminum-Copper 2014	3	21*21cm	1.0000	1cm, 2cm, and 3cm
Aluminum-Copper 2014	3	21*16cm	1.3334	1cm, 2cm, and 3cm
Aluminum-Copper 2014	3	21*11cm	2.0000	1cm, 2cm, and 3cm

Table (3) Aluminum-Alloy Plates Specifications

Grid Specifications	
Dimensions	$20mm * 20mm$
Spacing Between Each Grid Line	$1mm$
Depth of the Grid Line	$0.001mm$
Width of the Grid Line	$0.1mm$
Crack Specifications	
Crack Type	Surface Crack
Crack Position	Centered Crack
Crack Depth	$2mm$

Table (4) The-Engraved-Cracks-and-Grids Specifications.

X(mm)	Y(mm)	U_x(μm)	U_y(μm)
0	0	0	0
4	0	264	0
8	0	373	0
12	0	457	0
16	0	528	0
20	0	590	0
0	2	264	267
4	2	300	71
8	2	387	48
12	2	465	38
16	2	533	33
20	2	594	30
0	4	373	378
4	4	375	157
8	4	425	101
12	4	487	80
16	4	548	68
20	4	605	60
0	6	458	463
4	6	452	245
8	6	475	160
12	6	520	124
16	6	571	104
20	6	622	92
0	8	528	535
4	8	522	326
8	8	530	222
12	8	560	171
16	8	601	143
20	8	645	125
0	10	591	598
4	10	585	400
8	10	586	285
12	10	604	221
16	10	635	184
20	10	672	160
Plastic Zone Size		2.50mm	
Crack Extension		11mm	

Table (A1) The Experimental Output Data for 10mm-Crack-Length and 1-Aspect-Ratio Pure Aluminum 1100 Thin Plate